Supporting Information for

High-Defect-Density Graphite for Superior-Performance Aluminum-Ion Batteries with Ultra-Fast Charging and Stable Long Life

Jisu Kim[1], Michael Ruby Raj[1], and Gibaek Lee[1,*]

[1]Advanced Energy Materials Design Lab, School of Chemical Engineering, Yeungnam University, 38541 Gyeongsan, Republic of Korea

*Corresponding author.
E-mail: gibaek@ynu.ac.kr (Gibaek Lee)

S1. Experimental Section

Calculation method for the degree of graphitization.

The degree of graphitization (DG) of graphite can be defined as the level of the transformation of non-graphitic carbon material into a well-ordered graphitic structure. DG can be calculated from the following equation [S1]:

$$\text{DG (\%)} = \frac{0.3440 - d(002)}{0.3440 - 0.3354} \times 100 \quad (1)$$

where 0.3440 nm is the *d*-spacing of the fully non-graphitized carbon (nm), 0.3354 nm is the *d*-spacing of the ideal graphite crystallite (nm), and $d_{(002)}$ is the *d*-spacing derived from the XRD pattern of the studied materials (PG, AEG and BEG).

Calculation methods of energy density and power density.

We have calculated using modified equation as per earlier report [S2-S4]. Specific energy density (E_{sp}) and power density (P_{sp}) of the BEG was calculated using following equation.

$$E_{sp} = \frac{V \times I \times t}{m} \ (Wh\ kg^{-1}) \quad (2)$$

$$P_{sp} = \frac{V \times I}{m} \ (W\ kg^{-1}) \quad (3)$$

Where V is the operating voltage, I is the current (A), t is the time of the discharge cycle (h), m is the loading mass of cathode active material (kg).

S2. Supplementary Figures and Tables

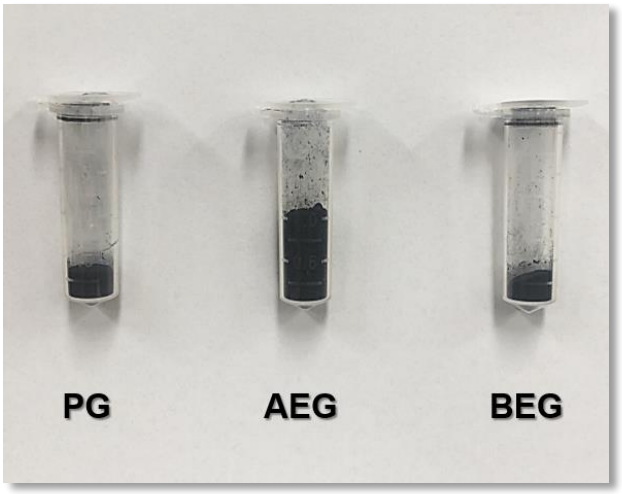

Fig. S1 Optical images of 0.1 g samples of PG, AEG, and BEG.

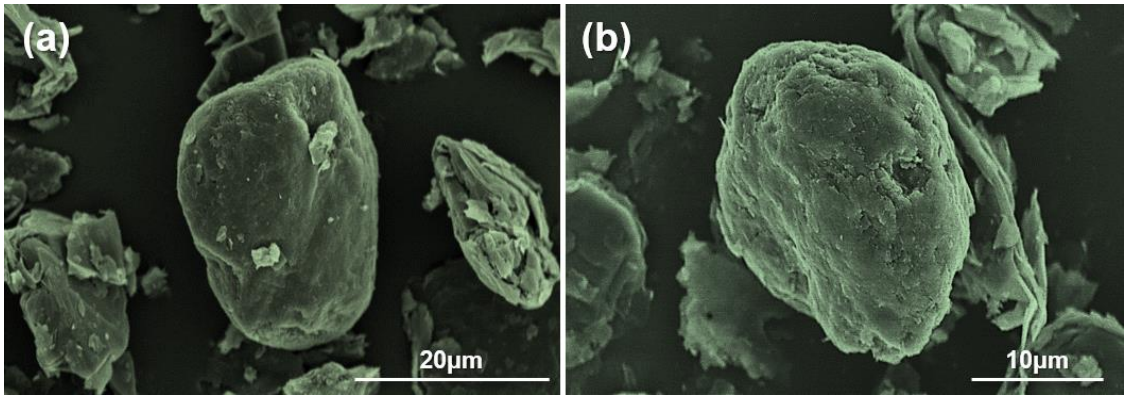

Fig. S2 a and **b** Low-resolution SEM images for potato-shaped PG specimen.

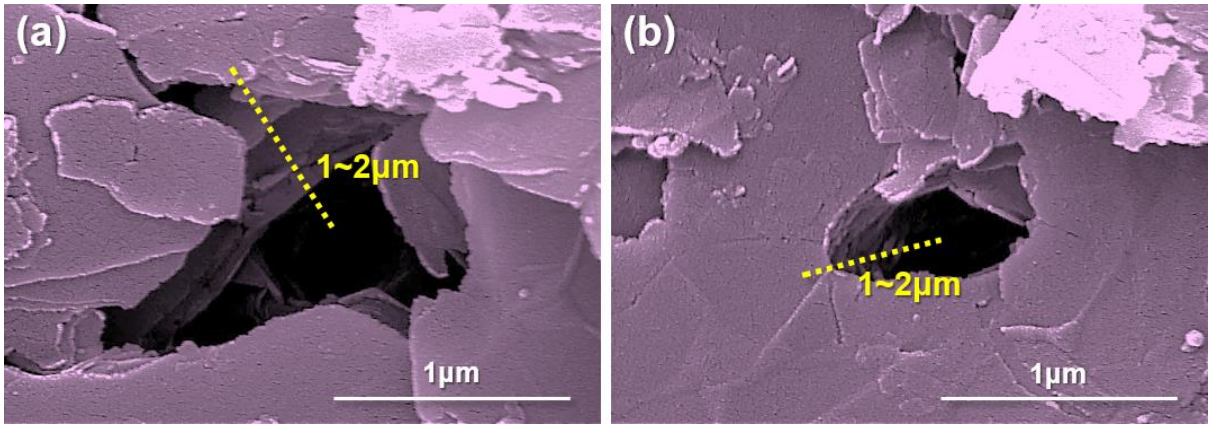

Fig. S3 a and **b** SEM images of the KOH-etched graphite (BEG). BEG surface comprise large size of 1~2 μm deep holes with approximately 8~10 graphite layers, which could facilitate the penetration of large volume of ionic liquid and more $AlCl_4^-$ ions within the BEG rather than only surface of BEG.

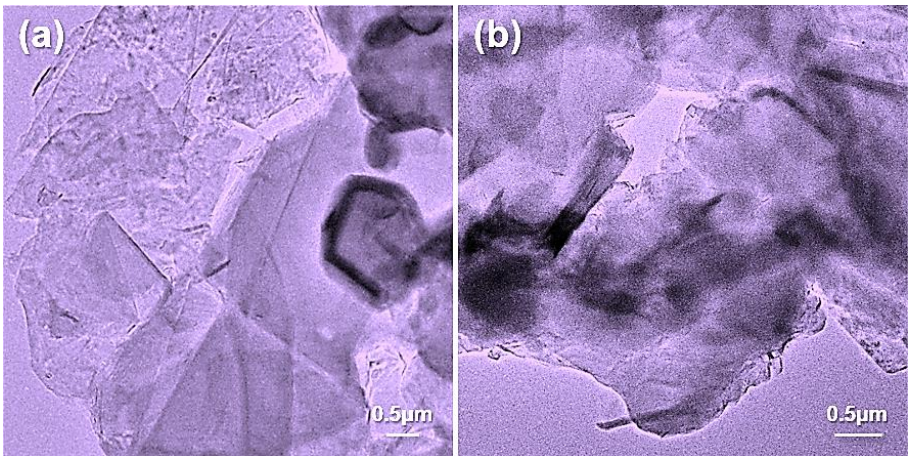

Fig. S4 a and **b** TEM images of BEG. The pores/holes are about 500 nm in size.

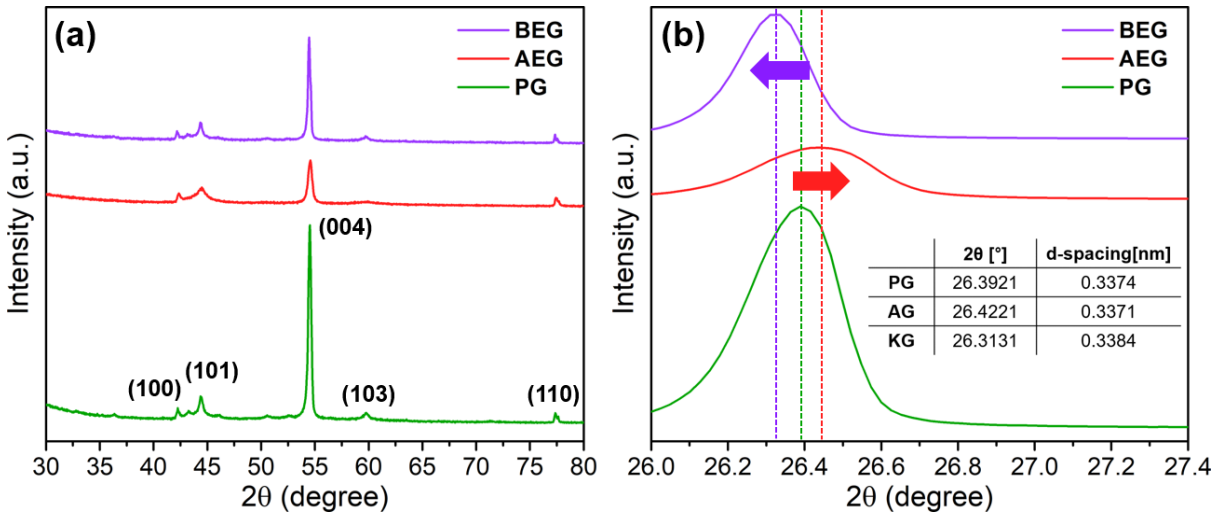

Fig. S5 XRD pattern **a** from 30–80 °and **b** the enlarged spectrum for the (002) plane peak of three specimens.

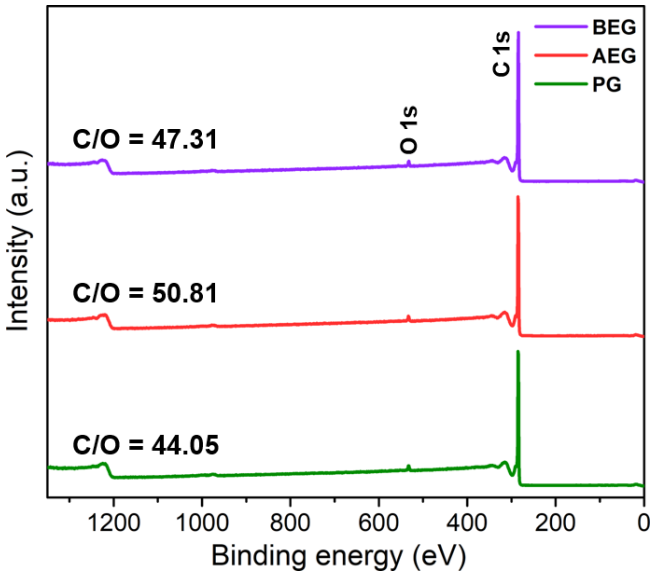

Fig. S6 XPS survey spectra of PG, AEG and BEG with ratio of C and O elements.

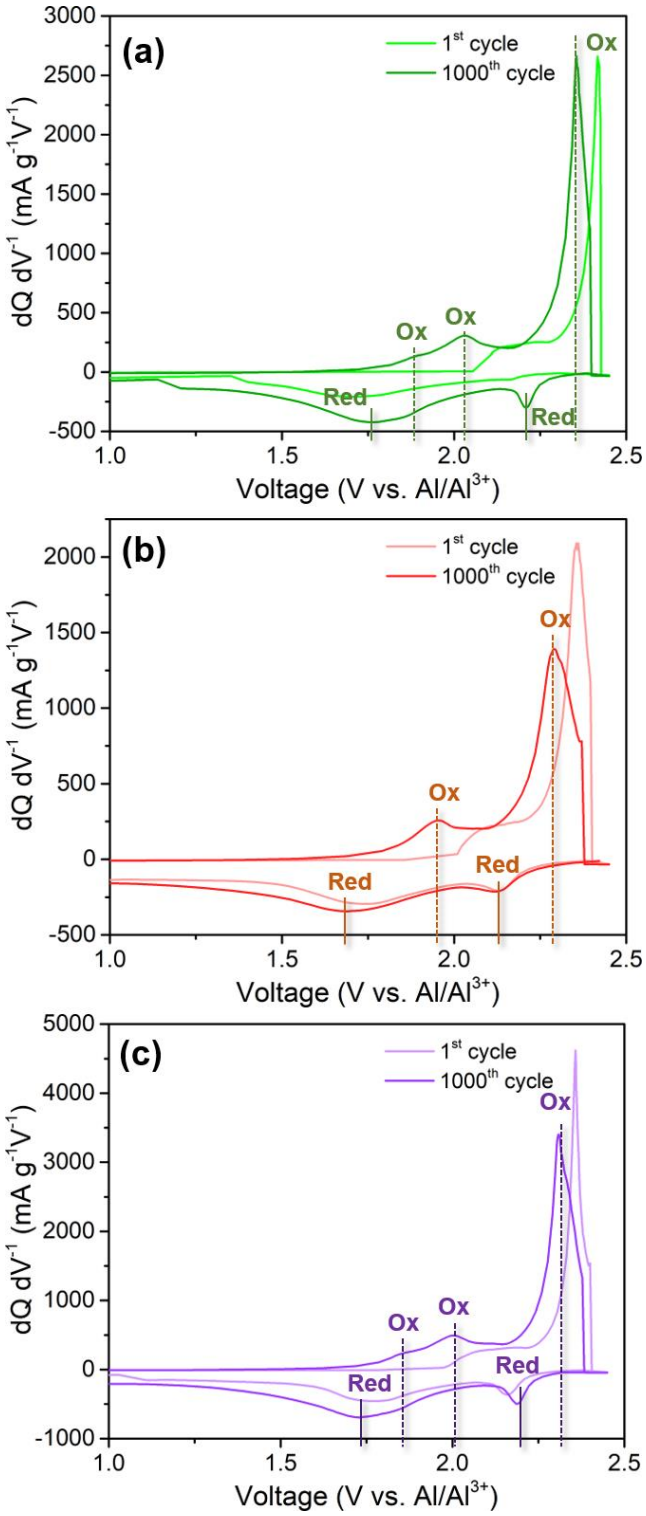

Fig. S7 Differential capacity–voltage (dQ/dV) profile for **a** PG, **b** AEG, and **c** BEG.

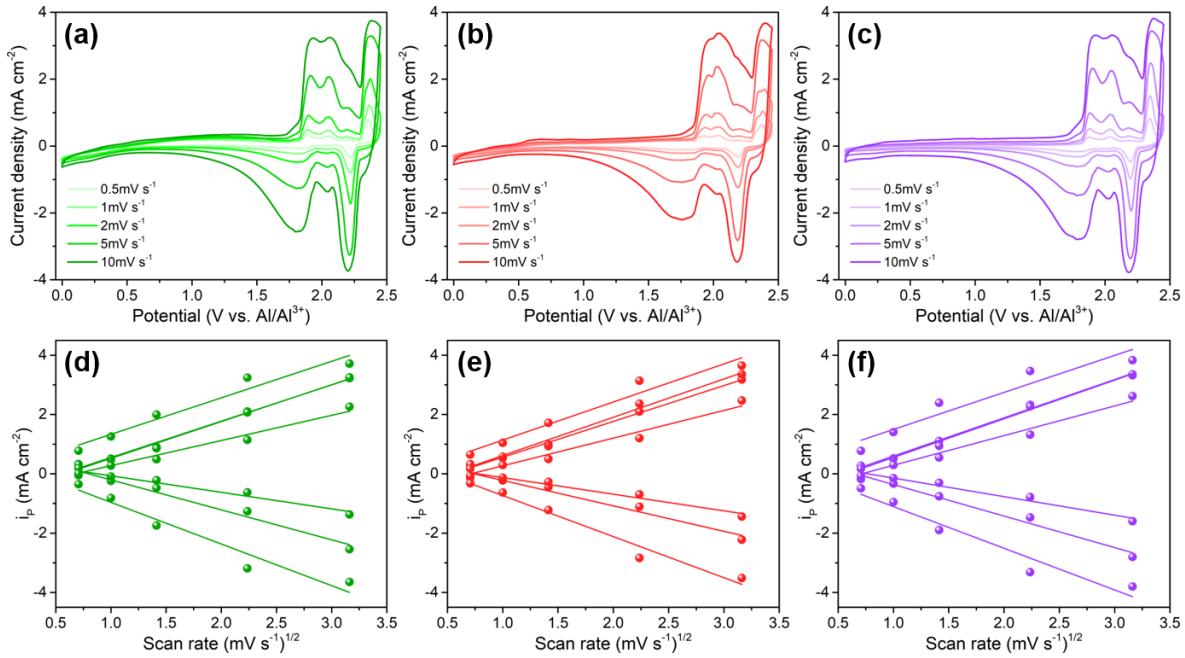

Fig. S8 CV curves at different scan rates of **a** PG, **b** AEG, and **c** BEG. **d–f** Relationship between square root of scan rate ($v^{1/2}$) and peak current (i_p) of each specimens.

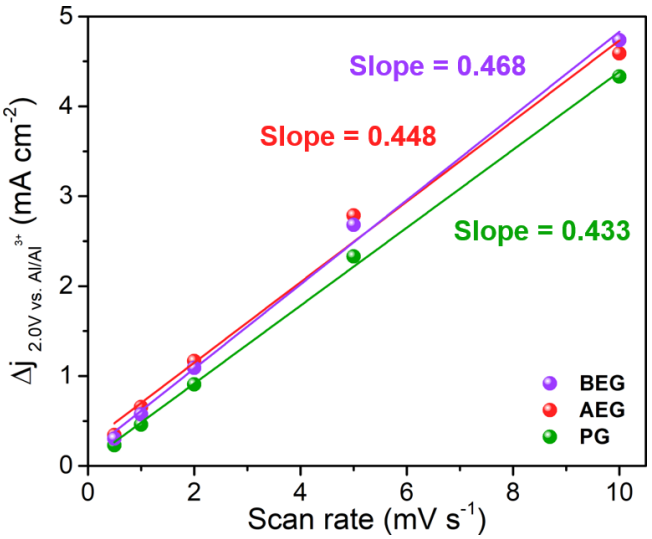

Fig. S9 Relationship between scan rate and distances in current density variation ($\Delta j = j_a - j_c$) at a potential of 2.0 V. The linear slope is the double layer capacitance (C_{dl}) of the specimens and can be used to calculate the relative electrochemically active surface area.

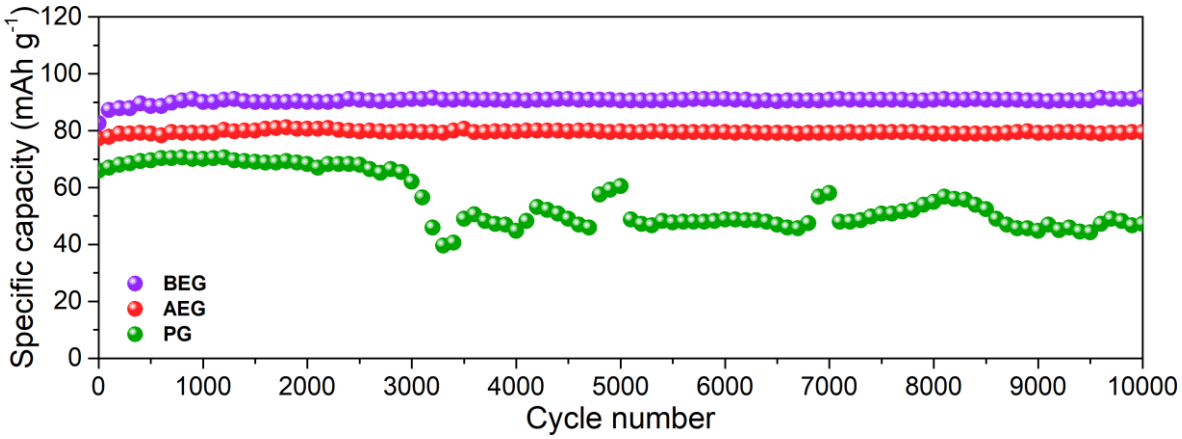

Fig. S10 Ultralong-term cyclic stability of PG, AEG and BEG at an ultra-high current density of 10 A g^{-1} over 10000 cycles.

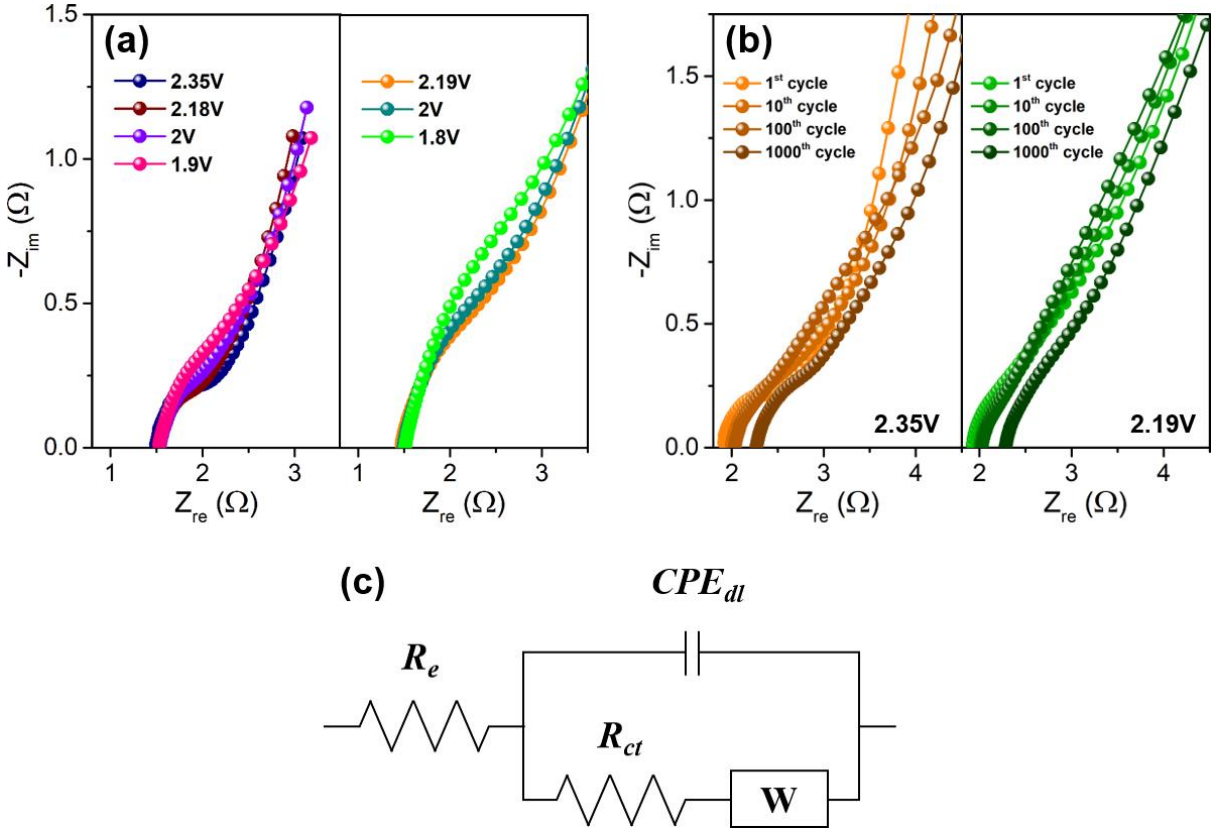

Fig. S11 Two-dimensional Nyquist plot of **a** various oxidation potentials (intercalation) and reduction potentials (de-intercalation); **b** 1st cycle →1000 cycled BEG at oxidation potential of 2.35 V and reduction potential of 2.19 V. **c** Equivalent circuit corresponding **a** and **b**.

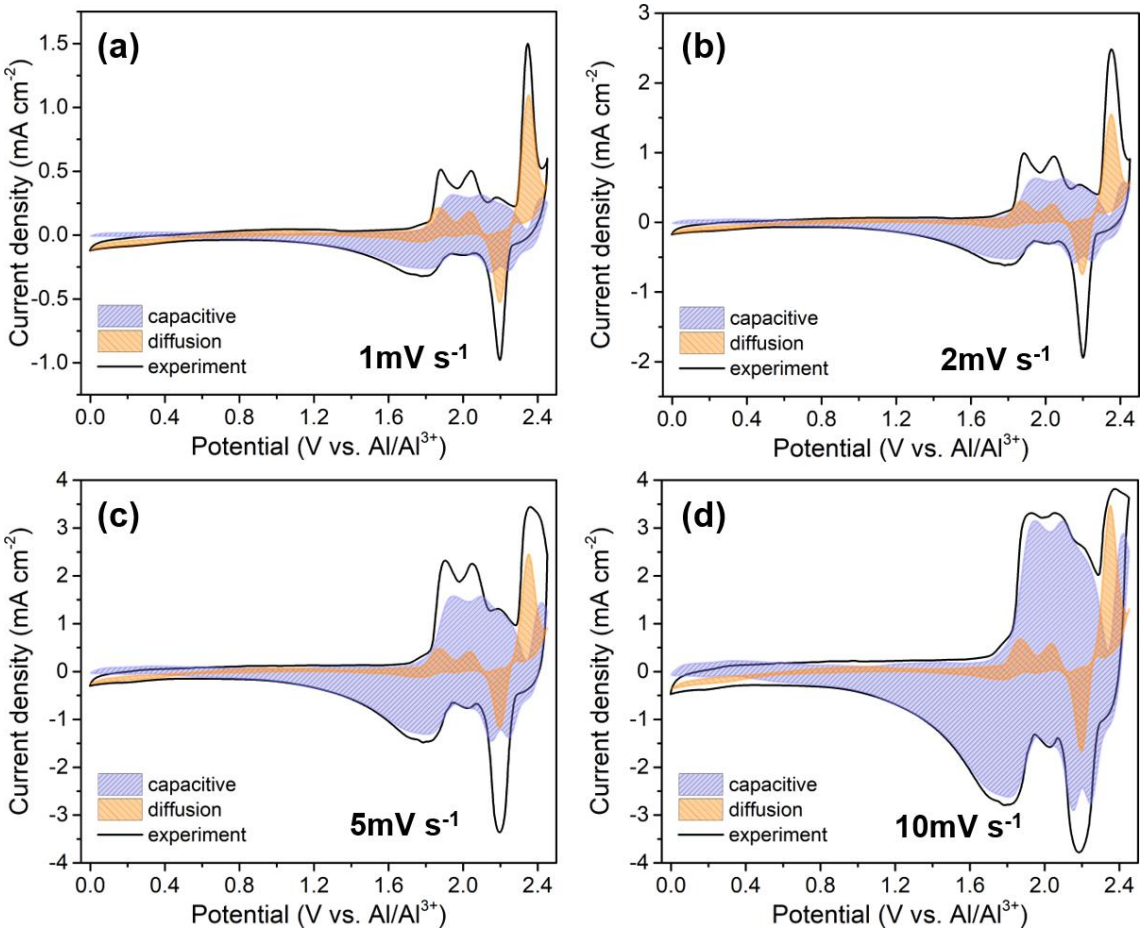

Fig. S12 Capacitive- and diffusion-controlled contribution curves of BEG at a scan rate of **a** 1 mV s^{-1}, **b** 2 mV s^{-1}, **c** 5 mV s^{-1}, and **d** 10 mV s^{-1}.

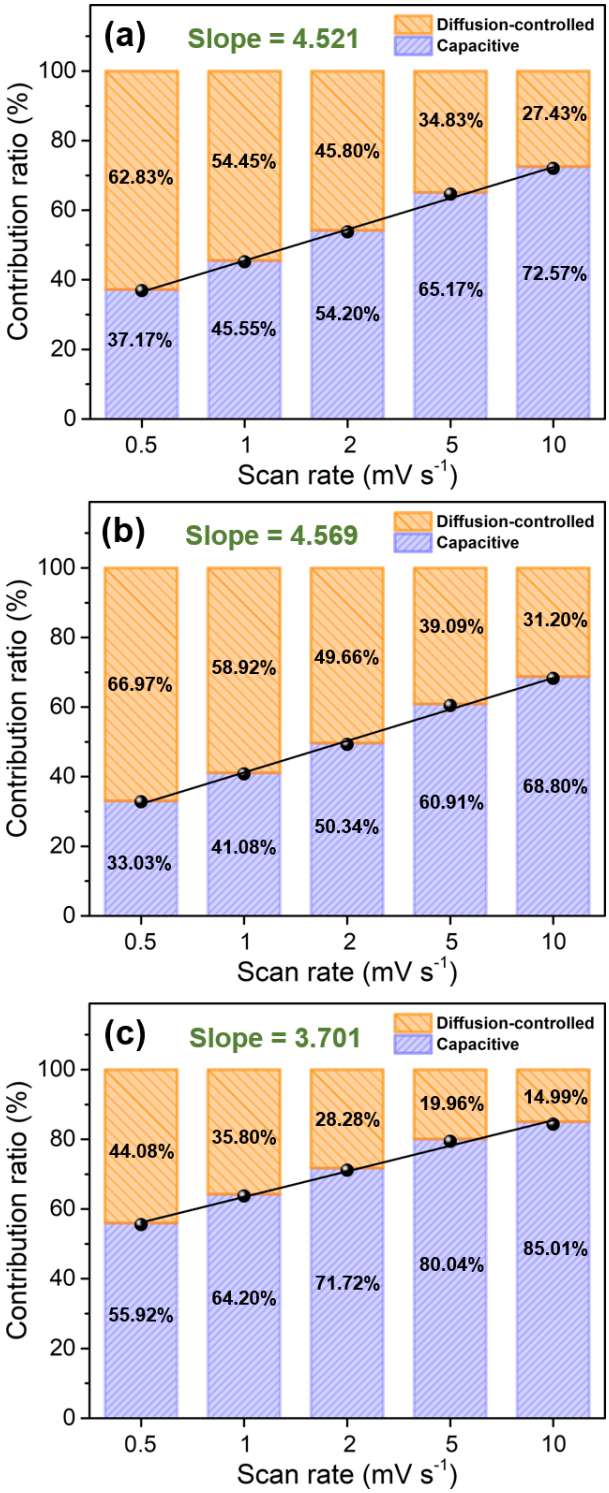

Fig. S13 Total contribution ratios of capacitive and diffusion: **a** PG, **b** AEG, and **c** BEG.

Table S1 Summary of diffusion coefficient (D_o) values for different redox peaks for PG, AEG, and BEG specimens.

$\times 10^{-6}$	Oxidation potentials				Reduction potentials		
	1.9 V	**2.0 V**	**2.2 V**	**2.35 V**	**1.8 V**	**2.0 V**	**2.2 V**
PG	5.10	5.27	2.42	5.19	3.50	1.04	6.72
AEG	5.02	5.71	2.97	5.62	2.54	1.08	6.53
BEG	5.71	5.80	3.43	5.36	3.85	1.36	6.82

Table S2 Comparison for the $AlCl_4^-$ Diffusivities (*D)* of our materials (PG, AEG and BEG) with bulk graphite and few-layer graphene films.

System	*N*	*D* ($cm^2 s^{-1}$)	$D/D_{graphite}$	Ref
Bulk graphite	–	2.2×10^{-9}	1.0	[S5]
Few-Layer Graphene Films (graphitic foam)	6	3.3×10^{-9}	1.5	[S5]
	5	2.3×10^{-8}	10.2	
	4	1.1×10^{-7}	47.8	
	3	3.4×10^{-7}	153.2	
	2	5.0×10^{-7}	225.2	
PG	–	5.27×10^{-6}	2395.4	This work
AEG	–	5.71×10^{-6}	2595.4	
BEG	–	5.80×10^{-6}	2636.3	

**N* represents the number of layers in graphene film.

Table S2 summarizes the absolute and relative $AlCl_4^-$ ion diffusivities with respect to bulk graphite and few-layer of graphene films (graphitic foam). It can been seen that $AlCl_4^-$ diffusivity increased markedly as the number of graphene layers decreased in graphitic foam [S5]. The diffusivity in the five-layer graphene film (2.3×10^{-8} cm^2 s^{-1}) is 10.2 times faster than that in bulk graphite (2.2×10^{-9} cm^2 s^{-1}), indicating that $AlCl_4^-$ ion diffusivity increased in graphitic foam from five to two graphene layers. The following trend, the $AlCl_4^-$ diffusivities in PG (5.27×10^{-6} cm^2 s^{-1}), AEG (5.71×10^{-6} cm^2 s^{-1}) and BEG (5.80×10^{-6} cm^2 s^{-1}) are approximately 2390 to 2640 times faster than that of the bulk graphite. This result manifesting the high $AlCl_4^-$ diffusivities (ionic conductivity) of PG, AEG and BEG compared to that of bulk graphite [S5]. Hence, it is interpreted that the experimentally observed the diffusion coefficient ($AlCl_4^-$ diffusivities) with respect to diffusion rate in PG, AEG and BEG cathode are greater than that of bulk graphite and graphitic foam.

Table S3 Summary of EIS results for BEG cathode at all redox peaks before cycling.

[Ω]	Oxidation potentials				Reduction potentials		
	1.9 V	2.0 V	2.18 V	2.35 V	1.8 V	2.0 V	2.19 V
R_e	1.53	1.53	1.53	1.49	1.51	1.49	1.47
R_{ct}	1.42	1.07	1.02	0.91	3.49	2.53	2.50

Table S4 Comparison of power density and energy density for AEG and BEG electrodes with other graphitic carbon materials.

Cathode materials	Power density [W kg^{-1}]	Energy density [Wh kg^{-1}]	Refs.
Graphitic foam	~3,000	~40	[S6]
Mesoporous rGO powder	21,000	170	[S7]
Kish graphite flakes	4,363	65	[S8]
Defect-free graphene	30,000	60	[S9]
Small flake natural graphite	489	62	[S10]
Zeolite-template carbon	290	64	[S11]
Graphite	–	135	[S19]
Vein graphite	–	59.1	[S21]
Base-etched graphite (BEG)	**2,680**	**282.98**	**This work**
	13,583	**268.03**	
	15,903	**265.04**	
	44,497	**247.21**	
	75,058	**208.50**	
Acid-treated expanded graphite (AEG)	**2,453**	**252.84**	
	9,830	**226.63**	
	12,431	**220.99**	
	24,434	**200.90**	
	49,124	**161.70**	

Table S5 Comparison of the electrochemical performance for AEG and BEG electrodes with the previously reported state-of-the-art graphitic carbon materials.

Cathode materials	Electrolyte	Capacity [mAh g^{-1}] / current density [mA g^{-1}]	Cycle	Potential window [V]	Coulombic efficiency [%]	Ref.
Base-etched graphite (BEG)	**$AlCl_3$:[EMIm]Cl = 1.5:1**	**~ 110 / 4,000**	**1,000**	**0.0-2.45**	**99.9**	**This work**
		~ 91 / 10,000	**10,000**			
Acid-treated expanded graphite (AEG)		**~ 89 / 4,000**	**1,000**		**99.1**	
		~ 80 / 10,000	**10,000**			
Graphitic foam	$AlCl_3$:[EMIm]Cl = 1.3:1	~ 66 / 66	200	0.0-2.5	~ 99.3	[S6]
		~ 60 / 4,000	7,500			
Mesoporous rGO powder	$AlCl_3$:[EMIm]Cl = 1.3:1	~ 150 / 100	100	0.01-2.2	~ 85	[S7]
		~ 100 / 1,000	3,000			
		~ 55 / 10,000	25,000			
Kish graphite flakes	$AlCl_3$:[EMIm]Cl = 1.5:1	120 / 500	200	0.01-2.45	~ 80	[S8]
Defect free graphene	$AlCl_3$:[EMIm]Cl = 1.3:1	100 / 5,000	25,000	0.7-2.51	~ 97	[S9]
Small flake natural graphite	$AlCl_3$:[EMIm]Cl = 2:1	132 / 100	100	0.5-2.4	92	[S10]
Zeolite-templated carbon	$AlCl_3$:[EMIm]Cl = 1.3:1	~ 180 / 100	500	0.01-2.2	98–100	[S11]
		~ 157 / 1,000	1,000			
Natural graphite flake	$AlCl_3$:[EMIm]Cl = 1.3:1	100 / 198	1,100	0.5-2.45	~ 99	[S12]
		60 /660	6,000			
High purity graphite paper	$AlCl_3$:[EMIm]Cl = 1.3:1	~ 70 / 20	600	0.5-2.4	~ 98	[S13]
		~ 70 / 50	200			

Cathode materials	Electrolyte	Capacity [mAh g^{-1}] / current density [mA g^{-1}]	Cycle	Potential window [V]	Coulombic efficiency [%]	Ref.
Expanded graphite	$AlCl_3$:[EMIm]Cl = 1.3:1	~ 60 / 1,000	3,000	0.7-2.51	69.8	[S14]
		~ 60 / 5,000	10,000			
	$AlCl_3$:ET* = 1.5:1	~ 98 / 1,000	5,000	0.7-2.54	77.5	
		~ 78 / 5,000	30,000			
3D graphene mesh network	$AlCl_3$:[EMIm]Cl = 1.3:1	57 / 240	200	0.0-2.5	97.5	[S15]
Large-sized few-layer graphene	$AlCl_3$:[PMIm]Cl = 1.3:1	~ 90 / 60	200	0.0-2.5	~ 95	[S16]
		~ 80 / 300	4,500			
Graphite powder	$AlCl_3$:[EMIm]Cl = 1.3:1	~ 73 / 100	180	1.0-2.2	~ 99.7	[S17]
Trihigh tricontinuous (3H3C) graphene film	$AlCl_3$:[EMIm]Cl = 1.3:1	~ 120 / 6,000	16,000	0.6-2.5	~ 91.7	[S18]
		~120 / 100,000	250,000			
Graphite	$AlCl_3$:Urea = 1.5:1	50 / 2,000	8,000	0.3-2.4	~95	[S19]
Surface-perforated graphene	$AlCl_3$:[EMIm]Cl = 1.3:1	~197 / 2,000	200	0.5-2.4	92.5	[S20]
		~147 / 5,000	1,000			
Vein graphite flake	$AlCl_3$:[EMIm]Cl = 2.1:1	103 / 100	50	0.01-2.38	80-90	[S21]
		~90 / 500	100			
Graphite	$AlCl_3$:[EMIm]Cl = 1.5:1	~110 / 200	100	0.4-2.4	88-90	[S22]

*ET = triethylamine hydrochloride

Table S6 Comparison of different technologies (methods) for adequate surface defects and their specific capacities.

Cathode materials	Technologies	Surface defects	Specific Capacity / Current rate	Ref.
Acid expanded graphite (AEG)	**Acid (sulfuric/nitric acid) mixing process**	**Expanded the graphitic layers**	**~89 mAh g^{-1} / 4,000 mA g^{-1}**	**This work**
Base etched graphite (BEG)	**Base (4M KOH) etching process**	**Expanded layers and Pores/holes on the graphite surface**	**~110 mAh g^{-1} / 4,000 mA g^{-1}**	
Mesoporous rGO powder	Hummer method	Large defect and pores	~100 mAh g^{-1} / 1,000 mA g^{-1}	[S7]
Kish graphite flakes	Sonication	Crater morphology with deep craters(holes)	120 mAh g^{-1} / 500 mA g^{-1}	[S8]
Defect-free graphene	High temperature annealing (>2000℃)	Vacancy holes and polygons	100 mAh g^{-1} / 5,000 mA g^{-1}	[S9]
Zeolite-templated carbon	Impregnation of ion exchanged zeolite Y	High pore-to-pore regularity & high surface area	157 mAh g^{-1} / 1,000 mA g^{-1}	[S11]
Natural graphite flake	Casting and etching	Free-standing surface	60 mAh g^{-1} / 660 mA g^{-1}	[S12]
3D graphene mesh network	Electroplating and etching	3D mesh network	57 mAh g^{-1} / 240 mA g^{-1}	[S15]
Trihigh tricontinuous (3H3C) graphene film	High temperature annealing	Honeycomb atomic lattice	~120 mAh g^{-1} / 6,000 mA g^{-1}	[S18]
Vein graphite flake	ultrasonication	Fragmentized particles	103 mAh g^{-1} / 100 mA g^{-1}	[S21]
Graphene nanoribbons porous 3D graphene (GNHPG)	Plasma-etching	Nanovoids distributed on the 3D graphene	123 mAh g^{-1} / 5,000 mA g^{-1}	[S23]

Supplementary References.

[S1] K. V. Kravchyk and M. V. Kovalenko, Adv. Energy Mater. **9**, 1901749 (2019).

[S2] J. Kim, D. Lee, J. Lee, C. Kim, Sci. Rep. **10,** 15586 (2020).

[S3] Y. Lu, B. M. Gallant, D. G. Kwabi, J. R. Harding, R. R. Mitchell, M. S. Whittinghamd, S. Yang, Energy Environ. Sci. **6**(3), 750 (2013).

[S4] B. E. Conway, Electrochemical Supercapacitor 417-477 (1999).

[S5] S. C. Jung, Y.-J. Kang, D.-J. Yoo, J. W. Choi, Y.-K. Han, J. Phys. Chem. C **120**(25), 13384−13389 (2016).

[S6] M. C. Lin, M. Gong, B. Lu, Y. Wu, D. Y. Wang, M. Guan, M. Angell, C. Chen, J. Yang, B. J. Hwang, H. J. Dai, Nature **520**, 324-328 (2015).

[S7] J. Smajic, A. Alazmi, N. Batra, T. Palanisamy, D. H. Anjum, P. M. F. J. Costa, Small **14**(51), 1803584 (2018).

[S8] S. Wang, K. V. Kravchyk, F. Krumeich, M. V. Kovalenko, ACS Appl. Mater. Inter. **9**(34), 28478-28485 (2017).

[S9] H. Chen, F. Guo, Y. Liu, T. Huang, B. Zheng, N. Ananth, Z. Xu, W. Gao, C. Gao, Adv. Mater. **29**(12) 1605958 (2017).

[S10] K. V. Kravchyk, S. Wang, L. Piveteau, M. V. Kovalenko, Chem. Mater. **29** (10), 4484-4492 (2017).

[S11] N. P. Stadie, S. Wang, K. V. Kravchyk, M. V. Kovalenko, ACS Nano **11**(2), 1911-1919 (2017).

[S12] D. Y. Wang, C. Y. Wei, M. C. Lin, C. J. Pan, H. L. Chou, H. A. Chen, M. Gong, Y. Wu, C. Yuan, M. Angell, Y. J. Hsieh, Y. H. Chen, C. Y. Wen, C. W. Chen, B. J. Hwang, C. C. Chen, H. Dai, Nature Commun. **8**, 14283 (2017).

[S13] S. Wang, S. Jiao, W. Song, H. Chen, J. Tu, D. Tian, H. Jiao, C. Fu, D. Fang, Energy storage mater. **12**, 119-127 (2018).

[S14] X. Dong, H. Xu, H. Chen, L Wang, J Wang, W. Fang, C. Chen, M. Salman, Z. Xu, C. Gao, Carbon **148**, 134-140 (2019).

[S15] G. Y. Yang, L. Chen, P. Jiang, Z. Y. Guo, W. Wang, Z. P. Liu, RSC Adv. **6**(53), 47655-47660 (2016).

[S16] L. Zhang, L. Chang, H. Luo, X. Zhou, Z. Liu, Adv. Energy Mater. **7**(15), 1700034 (2017).

[S17] M. Angell, C. Pan, Y. Rong, C. Yuan, M. Lin, B. Hwang, H. Dai, PNAS **14**(5), 834-839 (2017).

[S18] H. Chen, H. Xu, S. Wang, T. Huang, J. Xi, S. Cai, F. Guo, Z. Xu, W. Gao, C. Gao, Sci. Adv. **3**(12), eaao7233 (2017).

[S19] F. Jach, M. Wassner, M. Bamberg, E. Brendler, G. Frisch, U. Wunderwald, J. Friedrich, ChemElectroChem **8**, 1988-1992 (2021).

[S20] Y. Kong, Ch. Tang, X. Huang, A.K. Nanjundan, J. Zou, A. Du, C. Yu, Adv. Funct. Mater. **31**, 2010569 (2021).

[S21] S. Wang, M.V. Kovalenko, K.V. Kravchyk, Batter. Supercaps. **4**, 929-933 (2021).

[S22] G.A. Elia, K. Hoeppner, R. Hahn, Batter. Supercaps. **4**, 368-373 (2021).

[S23] X. Yu, B. Wang, D. Gong, Z. Xu, B. Lu, Adv. Mater. **29**(4), 1604118 (2017).